

Color projector light intensity adaptive high dynamic range 3D measurement method

HUANG Hao-zhen, NIU Bin, CHENG Shen, QU Xing-hua, ZHANG Fu-min

Citation:

HUANG Hao-zhen, NIU Bin, CHENG Shen, QU Xing-hua, ZHANG Fu-min. Color projector light intensity adaptive high dynamic range 3D measurement method[J]. *Chinese Optics*, 2025, 18(5): 1219–1229. doi: 10.37188/CO.EN-2024-0038

黄浩珍, 牛斌, 程深, 曲兴华, 张福民. 彩色投影仪光强自适应高动态范围三维测量方法[J]. *中国光学*, 2025, 18(5): 1219–1229. doi: 10.37188/CO.EN-2024-0038

View online: <https://doi.org/10.37188/CO.EN-2024-0038>

Articles you may be interested in

[Dynamic 3D measurement error compensation technology based on phase-shifting and fringe projection](#)

基于相移条纹投影的动态3D测量误差补偿技术

Chinese Optics. 2023, 16(1): 184 <https://doi.org/10.37188/CO.EN.2022-0004>

[3D small-field surface imaging based on microscopic fringe projection profilometry: a review](#)

显微条纹投影小视场三维表面成像技术综述

Chinese Optics. 2021, 14(3): 447 <https://doi.org/10.37188/CO.2020-0199>

[Three-dimensional measurement method of highly reflective surface based on per-pixel modulation](#)

逐像素调制的高反光表面三维测量方法

Chinese Optics. 2022, 15(3): 488 <https://doi.org/10.37188/CO.2021-0220>

[Projector calibration based on cross ratio invariance](#)

基于交比不变性的投影仪标定

Chinese Optics. 2021, 14(2): 320 <https://doi.org/10.37188/CO.2020-0111>

[Research progress of grating projection on machine 3D topography inspection technology](#)

光栅投影在机三维形貌检测技术研究进展

Chinese Optics. 2023, 16(3): 500 <https://doi.org/10.37188/CO.2022-0083>

[Laser intensity distribution measurement method based on tomographic imaging](#)

基于层析成像的激光强度分布测量方法

Chinese Optics. 2023, 16(4): 743 <https://doi.org/10.37188/CO.2022-0016>

Color projector light intensity adaptive high dynamic range 3D measurement method

HUANG Hao-zhen, NIU Bin, CHENG Shen, QU Xing-hua, ZHANG Fu-min*

(State Key Laboratory of Precision Measurement Technology and Instruments,
Tianjin University, Tianjin 300072, China)

* Corresponding author, E-mail: zhangfummin@tju.edu.cn

Abstract: The Fringe Projection Profilometry (FPP) system with a single exposure time or a single projection intensity is limited by the dynamic range of the camera, which can lead to overexposure and underexposure of the image, resulting in point cloud loss or reduced accuracy. To address this issue, unlike the pixel modulation method of projectors, we utilize the characteristics of color projectors where the intensity of the three-channel LED can be controlled independently. We propose a method for separating the projector's three-channel light intensity, combined with a color camera, to achieve single exposure and multi-intensity image acquisition. Further, the crosstalk coefficient is applied to predict the three-channel reflectance of the measured object. By integrating clustering and channel mapping, we establish a pixel-level mapping model between the projector's three-channel current and the camera's three-channel image intensity, which realizes the optimal projection current prediction and the high dynamic range (HDR) image acquisition. The proposed method allows for high-precision three-dimensional (3D) data acquisition of HDR scenes with a single exposure. The effectiveness of this method has been validated through experiments with standard planes and standard steps, showing a significant reduction in mean absolute error (44.6%) compared to existing single-exposure HDR methods. Additionally, the number of images required for acquisition is significantly reduced (by 70.8%) compared to multi-exposure fusion methods. This proposed method has great potential in various FPP-related fields.

Key words: fringe projection profilometry; crosstalk coefficient; optimal projection currents; high dynamic range

彩色投影仪光强自适应高动态范围三维测量方法

黄浩珍, 牛 斌, 程 深, 曲兴华, 张福民*

(天津大学 精密测试技术及仪器国家重点实验室, 天津 300072)

摘要:单一曝光时间或单一投影强度的条纹投影轮廓术 (FPP) 系统方法受限于相机的动态范围, 会导致图像的过饱和和欠饱和, 从而造成点云缺失或精度降低。为了解决这一问题, 有别于投影仪像素调制方法, 我们利用彩色投影仪三通道 LED 投影强度可单独控制的特点, 提出了投影仪三通道光强分离的方法, 结合彩色相机, 实现了单曝光、多光强图像采集。进一步地, 将串扰系数应用到被测物体三通道反射率预测中, 结合聚类与通道映射, 建立了投影仪三通道电流与相机三通道图像光强的像素级映射模型, 实现了最佳投影电流预测和高动态范围图像获取。我们所提出的方法只需一次曝光就能实现高动态范围场景的高精度三维数据获取, 该方法的有效性已通过标准平面和标准台阶的实验进行了验证, 相比于现有单曝光高动态范围方法显著降低了平均绝对误差 (44.6%), 相比于多曝光融合方法所需要的采集图像数量显著减小 (文中场景下图片数量减小 70.8%), 提出的方法在各种 FPP 相关领域具有巨大潜力。

关键词:条纹投影轮廓术; 串扰系数; 最佳投影电流; 高动态范围

中图分类号: TH741

文献标志码: A

doi: 10.37188/CO.EN-2024-0038

CSTR: 32171.14.CO.EN-2024-0038

1 Introduction

Fringe projection profilometry (FPP) is widely used in industrial measurement processes with the advantages of non-contact, high resolution, and high accuracy^[1-4]. However, limited by the dynamic range of the camera, the FPP system will be oversaturated and undersaturated when measuring complex objects with large variations in surface reflectance, resulting in large errors in the measurement results or even loss of measurement data^[5]. The task of achieving high-accuracy measurement of high dynamic range (HDR) targets in the field of 3D measurement has been one of the challenges in the optical measurement field^[6-7].

There are many methods to solve the high dynamic range scene, which are roughly divided into two types, one is to enhance the dynamic range by hardware^[8-11], for example, Huang *et al.* achieved HDR 2D image acquisition by adding digital micromirror devices^[10], and then combined with mask adaptive methods to achieve the acquisition of high-precision data for HDR 3D scenes. Although the reconstruction of HDR scene is achieved, it increases the cost of equipment and operation complexity. The other is to achieve high dynamic range by al-

gorithms, such as changing the exposure time of the camera^[5, 12-15], changing the brightness of the projector or the projection method^[6, 16-25]. For example, Zhang *et al.*^[15] proposed to extract high and low reflectivity regions from images with shorter and longer exposure times, respectively, by capturing a sequence of streaked images with different exposure times. This method effectively improves the dynamic range of the HDR target. In addition, the study of projector modulation is also a way to solve the issue, for example, Lin *et al.*^[20] marked the saturated regions in the image and then projected low-intensity stripe images onto these marked regions to achieve HDR measurements. There are also single-exposure solutions for high dynamics, such as Liu *et al.*^[26] who generated HDR streak maps for 3D reconstruction by projecting monochromatic light and separating the channels of a color image and then fusing them according to their intensities, which took advantage of the three-channel crosstalk of a color camera, but the method did not take into account the optimal intensities of three channels. In addition, deep-learning can also be used for high dynamic 3D reconstruction^[27-28], but the pre-training requires a large number of samples and the generalization ability is a worry. In conclusion, methods

based on multiple exposures and adaptive projection fringing are time inefficient, and additional auxiliary hardware to improve system performance adds cost and computational complexity.

We utilize the characteristic of a color projector where the three-channel projection intensity can be individually controlled, combined with a color camera, to propose a single-exposure HDR 3D shape measurement method based on adaptive modulation of the projector's current. The main contributions and innovations of this paper are as follows:

(1) A method for modulating the LED currents of a three-channel projector has been proposed, which simplifies the cumbersome processes of image loading and mapping associated with projector modulation. By leveraging the capability of the projector's three-channel light source to be independently controlled through LED currents, combined with a color camera, this approach enables single exposure multi-intensity image acquisition.

(2) A pixel-level mapping model has been proposed to relate the projector's three-channel light source current intensity to the image grayscale of a color camera under channel crosstalk conditions. This model enables the rapid computation of multi-channel reflectance in HDR scenes and facilitates the acquisition of the relationship model between projection current and image grayscale.

(3) An adaptive HDR three-dimensional imaging method has been proposed. By employing clustering segmentation to integrate the camera channels with the projection channels, this approach enables the prediction of optimal projection current and facilitates single-exposure 3D data acquisition in HDR scenes. Additionally, it achieves efficient and high-precision 3D measurement of complex reflectance objects.

2 Principle

Fig. 1 (color online) illustrates the system hardware and algorithm flow. It is a FPP measurement system consisting of a color projector and a color

camera. The three-channel projection intensity of the projector can be individually controlled by adjusting the LED intensity levels (0-255), with the LED current intensity being proportional to the projection intensity. First, the projector projects a uniform grayscale image, setting the current values for the red, green, and blue channels to (120, 120, 120) and (20, 20, 20) to obtain two pre-acquired images, as shown in Fig. 1(c). Next, three-channel separation and crosstalk correction of the joint pixels are performed from the two images to acquire three-channel crosstalk-free images (the calibration of the crosstalk function is demonstrated in Section 2.1), as shown in Fig. 1(d). HDR images are then calculated using the crosstalk-free images from each channel (Section 2.2), as shown in Fig. 1(b).

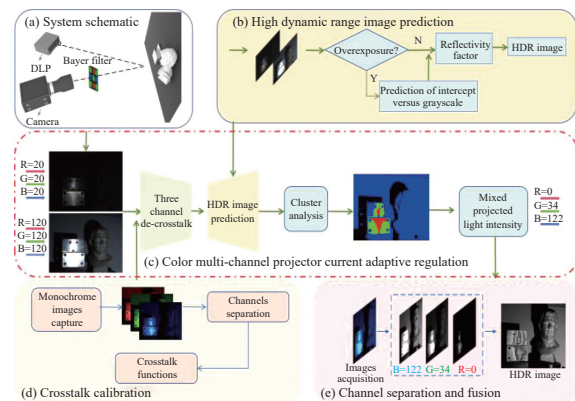


Fig. 1 Hardware and algorithm flowchart. (a) System schematic. (b) HDR image prediction. (c) Color multi-channel projector current adaptive modulation. (d) Crosstalk calibration process. (e) Color image channel separation and fusion

Subsequently, the obtained HDR images have background noise removed and undergo region segmentation using a clustering algorithm^[29], dividing the image into high-brightness, medium-brightness, and low-brightness regions, with each channel corresponding to different regions. This information is combined with crosstalk to calculate the optimal current intensity for the projector's three channels (Section 2.3). As shown in Fig.1(c), the projector's three-channel current intensity is calculated to (0,34,122), and images are captured by the camera. After separating the three channels of the acquired

image, they are fused according to the clustering mask to obtain a non-overexposed scene image, as shown in Fig. 1(e).

2.1 Crosstalk calculation

The existing crosstalk curve calibration method calculates the single-channel crosstalk function by projecting multiple uniform grayscale images with different intensities^[5]. To simplify the crosstalk calibration process, this paper proposes a rapid crosstalk calibration method, where single-channel crosstalk can be computed using just one image, and the mutual crosstalk among the three channels is quickly calibrated using three monochromatic images, as shown in Fig. 2 (color online).

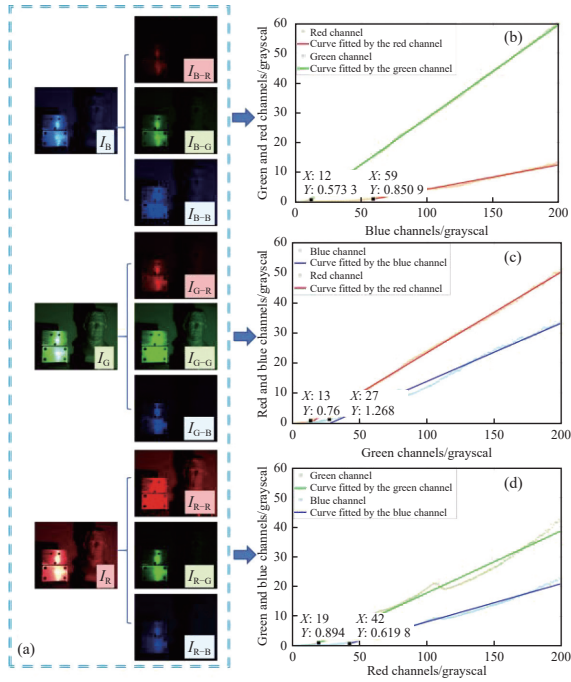


Fig. 2 Crosstalk calibration curve calculation. (a) Three-color image acquisition and channel separation. (b) Blue channel crosstalk fitting to green and red channels. (c) Green channel crosstalk fitting to blue and red channels. (d) Red channel crosstalk fitting to green and blue channels

First, the projector projects a uniform grayscale image, setting the currents of the three-color light sources to (100, 0, 0), (0, 100, 0), and (0, 0, 100) to acquire images I_R , I_G , and I_B from three channels, as shown in Fig. 2(a). The calibration of the channel crosstalk function is represented by Eq. (1).

$$\begin{cases} f_{R \rightarrow R}(I_{R_R}) = I_{R_R} \\ f_{R \rightarrow G}(I_{R_R}) = a_{R \rightarrow G} I_{R_R} + b_{R \rightarrow G} \\ \min \left(\sum (a_{R \rightarrow G} I_{R_R} + b_{R \rightarrow G} - I_{R_G})^2 \right) \\ f_{R \rightarrow B}(I_{R_R}) = a_{R \rightarrow B} I_{R_R} + b_{R \rightarrow B} \\ \min \left(\sum (a_{R \rightarrow B} I_{R_R} + b_{R \rightarrow B} - I_{R_B})^2 \right) \end{cases}, \quad (1)$$

where $I_{R \rightarrow R}$, $I_{R \rightarrow G}$, and $I_{R \rightarrow B}$ are the three-channel images after the separation of the I_R channel, as shown in Fig. 2(a). $f_{R \rightarrow R}$, $f_{R \rightarrow G}$, and $f_{R \rightarrow B}$ are the crosstalk functions of the red to the red, green, and blue channels as shown in Fig. 2(b), and $a_{R \rightarrow G}$, $b_{R \rightarrow G}$, $a_{R \rightarrow B}$, and $b_{R \rightarrow B}$ are the parameters of the crosstalk equations obtained from the fitting.

Similarly, the crosstalk function of the green channel to the three channels $f_{G \rightarrow R}$, $f_{G \rightarrow G}$, and $f_{G \rightarrow B}$, the crosstalk function of the blue channel to the three channels $f_{B \rightarrow R}$, $f_{B \rightarrow G}$, $f_{B \rightarrow B}$ can be obtained. The fitted curves are shown in Fig. 2(c) and Fig. 2(d), and the calibration results are shown in Table 1.

Tab. 1 Crosstalk calibration results

	$a_{\rightarrow R}$	$b_{\rightarrow R}$	$a_{\rightarrow G}$	$b_{\rightarrow G}$	$a_{\rightarrow B}$	$b_{\rightarrow B}$
R	1	0	0.209	3.081	0.129	4.789
G	0.268	3.307	1	0	0.193	5.537
B	0.082	3.995	0.314	3.194	1	0

2.2 HDR image calculation

The grayscale of the image is influenced by external lighting, camera gain, and the reflectivity of the object being captured^[10], which can be expressed by Eq. (2):

$$I(x, y; t) = \alpha \rho(x, y) I^p(x, y) + \alpha \rho(x, y) I^c(x, y) + I^n(x, y), \quad (2)$$

where $I(x, y; t)$ is the image brightness obtained by the camera at the pixel coordinates (x, y) for the exposure time t , α is the proportionality coefficient of the light intensity converted to grayscale values, $\rho(x, y)$ is the reflectivity of the illuminated object, $I^p(x, y)$ is the projector's light intensity on the object, $I^c(x, y)$ is the ambient light intensity on the surface of the object, and $I^n(x, y)$ is the noise from camera it-

self.

If $I^p(x,y)$ is known, and the exposure time is fixed, then $t\alpha$ is a constant value. Therefore, by projecting two images with known brightness levels using the projector and capturing two images with the camera, the reflectivity $\rho(x,y)$ of each pixel corresponding to the object within the camera's imaging range can be calculated. Assuming the projector's current intensities are set to 20 and 120 for uniform grayscale images (maximum grayscale value is 255), let these images be $I^{p20}(x,y)$ and $I^{p120}(x,y)$, and the captured image values be $I^{20}(x,y;t)$ and $I^{120}(x,y;t)$. Taking a scene that includes an aluminum metal workpiece and a plaster bust as an example, the captured images are shown in Fig. 3(a)

(color online). When $I^{120}(x,y;t) < T$, the relationship between projection brightness and image grayscale is linear. Let T be the minimum grayscale value in the saturated region of the image, set to $T=200$ to ensure the linear relationship. Reflectance factor $K(x,y)$ is $t\alpha\rho(x,y)$, the reflectivity coefficient $K(x,y)$ and the intercept $LB(x,y)$ are calculated as shown in Eq. (3), with the results displayed in the upper left in Fig. 3(b) (color online) at position b-1.

$$\begin{cases} Y(x,y) = K(x,y)I^p(x,y) + LB(x,y) \\ K(x,y) = \frac{I^{120}(x,y;t) - I^{20}(x,y;t)}{I^{p120}(x,y) - I^{p20}(x,y)} \\ LB(x,y) = I^{20}(x,y;t) - K(x,y)I^{p20}(x,y) \end{cases} \quad (I^{120}(x,y;t) < T) \quad (3)$$

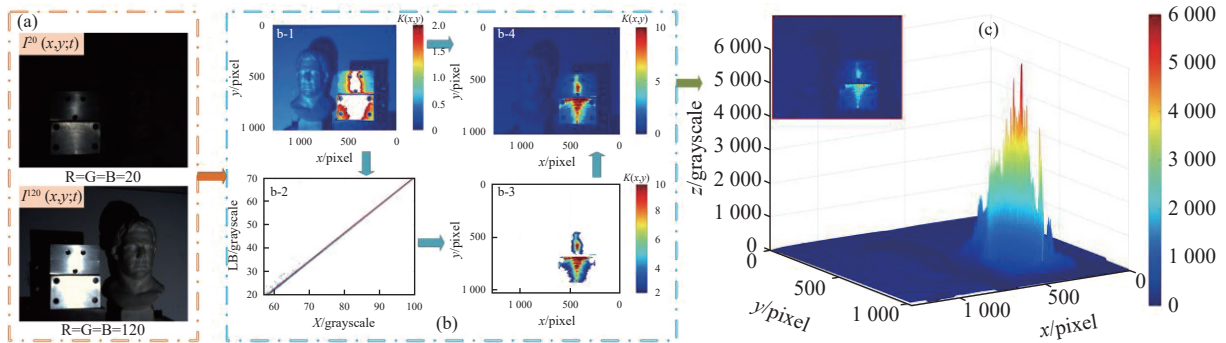


Fig. 3 HDR image calculation. (a) Pre-acquisition image. (b) Reflectance calculation of the measured scene, b-1 is the reflectance coefficient of the $I^{120}(x,y;t)$ non-over-exposed region, b-2 is the distribution and fitting result of $LB(x,y)$ and $I^{120}(x,y;t)$, b-3 is the reflectance coefficient of the $I^{120}(x,y;t)$ over-exposed region, and b-4 the reflectance coefficient of the measured scene. (c) High dynamic range measured scene data

When $I^{120}(x,y;t) < 255$, the reflection coefficients $K(x,y)$ and $LB(x,y)$ of the object's surface can be calculated using Eq. (3). However, when $I^{120}(x,y;t) \geq 255$, the reflection coefficient cannot be directly calculated. Therefore, the intercept $LB(x,y)$ is calculated through the pixel of $I^{120}(x,y;t) < 255$. The intercept $LB(x,y)$ is the effect of the external ambient light intensity and noise in the case that the projected current is 0, as shown in Eq. (4)

$$LB(x,y) = t\alpha\rho(x,y)I^c(x,y) + I^n(x,y) \quad (4)$$

In the underexposed region, $LB(x,y)$ is linearly related to $I^{20}(x,y;t)$. Therefore, the $LB(x,y)$ at $I^{120}(x,y;t) \geq T$ can be predicted by fitting the

relationship between $LB(x,y)$ and $I^{20}(x,y;t)$ at $I^{120}(x,y;t) < T$ as shown in Eq. (5). The results are shown in Fig. 3(b) at position b-2.

$$LB(x,y) = k_{LB}(x,y)I^{20}(x,y;t) + b_{LB}(x,y) \quad (5)$$

Where $k_{LB}(x,y)$ and $b_{LB}(x,y)$ are coefficients obtained by fitting. The reflectance coefficient $K(x,y)$ can be calculated by fitting the acquired $LB(x,y)$ as shown in Eq. (3), with the results displayed in Fig. 3(b) at position b-3.

$$K(x,y) = \frac{I^{20}(x,y;t) - LB(x,y)}{I^{p20}(x,y)} \quad (6)$$

When the current of the projector is n while projecting stripes, the reflectivity $I^n(x,y;t)$ can be

predicted from Eq. (7). The calculation results of the HDR image of the measured scene are displayed in Fig. 3(c).

$$I^n(x, y; t) = nK(x, y) + LB(x, y) \quad (7)$$

2.3 Optimal current prediction

There is a crosstalk between the channels of the pre-collected images. As shown in Fig. 4 (color online).

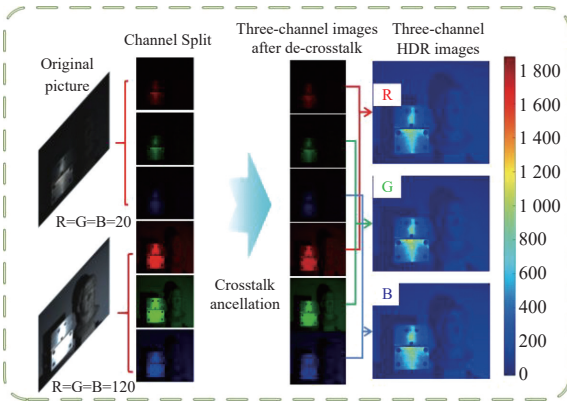


Fig. 4 Three-channel image crosstalk removal and three-channel HDR image acquisition

To accurately calculate the HDR images for each channel, it is necessary to correct for this crosstalk. Let the captured images be $I^{20}(x, y)$ and $I^{120}(x, y)$, and the separated images for the three channels be $I_R^{20}(x, y)$, $I_G^{20}(x, y)$, and $I_B^{20}(x, y)$. The crosstalk correction is shown in Eq. (8).

$$\begin{cases} I_R^{20} = f_{G \rightarrow R}(I_{Gv}^{20}) + f_{B \rightarrow R}(I_{Bv}^{20}) + I_{Rv}^{20} \\ I_G^{20} = f_{R \rightarrow G}(I_{Rv}^{20}) + f_{B \rightarrow G}(I_{Bv}^{20}) + I_{Gv}^{20} \\ I_B^{20} = f_{G \rightarrow B}(I_{Gv}^{20}) + f_{R \rightarrow B}(I_{Rv}^{20}) + I_{Bv}^{20} \end{cases}, \quad (8)$$

where I_{Rv}^{20} , I_{Gv}^{20} and I_{Bv}^{20} are the images after correction for crosstalk, similarly the three-channel separated image of $I^{120}(x, y)$ can be corrected, and the three-channel HDR image (as shown in the R, G,

$$\begin{cases} I_R^{nr} = f_{G \rightarrow R}(ng * \bar{K}_G + \bar{L}B_G) + f_{B \rightarrow R}(nb * \bar{K}_B + \bar{L}B_B) + nr * \bar{K}_R + \bar{L}B_R \\ I_G^{ng} = f_{R \rightarrow G}(nr * \bar{K}_R + \bar{L}B_R) + f_{B \rightarrow G}(nb * \bar{K}_B + \bar{L}B_B) + ng * \bar{K}_G + \bar{L}B_G \\ I_B^{nb} = f_{G \rightarrow B}(ng * \bar{K}_G + \bar{L}B_G) + f_{R \rightarrow B}(nr * \bar{K}_R + \bar{L}B_R) + nb * \bar{K}_B + \bar{L}B_B \end{cases} \quad (9)$$

where the values I_R^{nr} , I_G^{ng} , and I_B^{nb} correspond to the maximum target grayscale values in the three regions obtained from clustering segmentation, and to

and B images in Fig. 4 and Fig. 5, color online), reflection coefficients, and intercept coefficients (as shown in Eq. (7)) can be calculated by the method in Section 2.2.

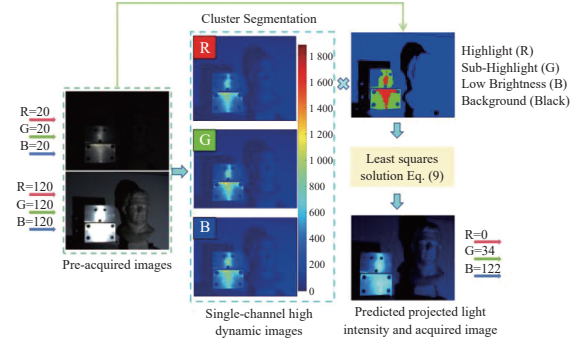


Fig. 5 Clustering and optimal light intensity calculation

The pre-acquired image is converted to grayscale by the method shown in Section 2.2 to obtain a HDR image. The image is divided into three parts by K-Means clustering segmentation, and the results are shown in Fig. 5. The R channel corresponds to the bright part, the G channel corresponds to the sub-bright part, the B corresponds to the low-bright part, and the black area in the figure is the part of the projected light that is blocked and is not involved in the calculation.

The reflectivity coefficient \bar{K}_R and intercept $\bar{L}B_R$ are obtained from the top 10 maximum values of the HDR image's red channel corresponding to the highlighted region.

The parameters \bar{K}_G , $\bar{L}B_G$, \bar{K}_B , and $\bar{L}B_B$ are obtained from the sub-highlighted and low-lighted regions. After correcting for crosstalk, the light intensity of the three separated channels of the images captured by the camera can be expressed as shown in Eq. (9).

ensure that they are not saturated, we set them all to 200. The values nr , ng , and nb represent the optimal projection current intensities for the three chan-

nels that need to be calculated. The optimal solution (0, 34, 122) is obtained by iteratively solving the system of equations in Eq. (9). After setting the projection currents, the images captured by the camera are shown in Fig. 5, and the non-saturated image obtained after fusing the three channels is displayed in Fig. 1(e).

3 Experiment

The hardware setup used in this paper is shown in Fig. 6 (color online). The system consists of a three-channel color projector (DLP4500) with a resolution of 912×1140 pixels and a color (RGB) camera with a resolution of 1280×1024 pixels. Projector led current module for the manufacturer encapsulated projection module, can individually control the three-channel projection current (0-255). The current and projection light intensity are approximately linearly related.

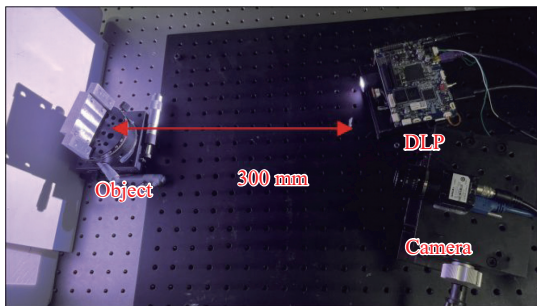


Fig. 6 Experiment setup

The camera has a focal length of 16 mm, and the working distance of the projector is 300 mm. During the measurement process, the projector projects a total of 12 sinusoidal encoded images with three frequencies and four steps (with pixel periods of 16, 18, and 21) onto the surface of the object. The camera then captures the modulated stripe images for phase unwrapping to obtain the absolute phase, which is used for subsequent 3D reconstruction.

The projector's three-channel currents are set to (0, 34, 122), and a color camera with a resolution of 1280×1024 pixels is used to capture the striped

images. The stripes used in this study are three-frequency sine stripes with a phase difference of 0.5π . The captured image is denoted as $I_i (i = 1, 2, 3 \dots 12)$, and the background intensity A can be calculated using Eq. (10).

$$A = \left(\sum_{i=1}^{12} I_i \right) / 12 \quad (10)$$

The process of calculating high dynamic range stripes for highly reflective objects is shown in Fig. 7 (color online). The background intensity A is separated into three channels to obtain A_r , A_g , and A_b .

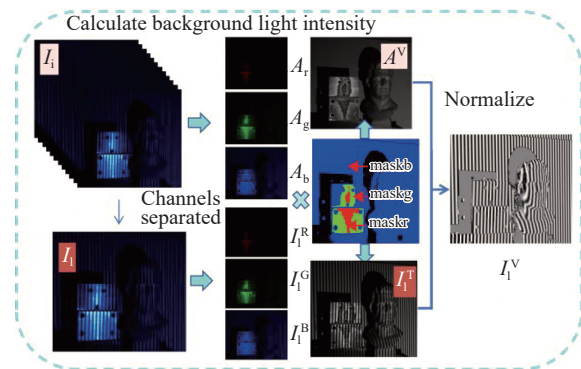


Fig. 7 High dynamic range streak acquisition for highly reflective objects

The normalized fused stripes are expressed as Eq. (11).

$$\begin{cases} A^V = A_r * mask_r + A_g * mask_g + A_b * mask_b \\ I_i^T = I_i^R * mask_r + I_i^G * mask_g + I_i^B * mask_b \\ I_i^V = (I_i^T - A^V) / (A^V + 0.001) * 0.5 + 0.5 \end{cases} \quad (11)$$

where I_i^T is the image obtained after fusing the three channels, I_i^R , I_i^G , and I_i^B are the images obtained after separating the three channels of I_i , A^V is the image obtained by fusing the background intensity across the three channels, and I_i^V is the normalized stripe image. The $mask_r$, $mask_g$, and $mask_b$ are the three-channel masks calculated from clustering segmentation, where the constant 0.001 is used to avoid division by zero.

As shown in Fig. 8 (color online), the 3D point cloud generated using the method described in this paper is shown in Fig. 8(b). Compared to the unpro-

cessed method (Fig. 8(a)), the point cloud in the overexposed areas has been completed, achieving HDR 3D data generation.

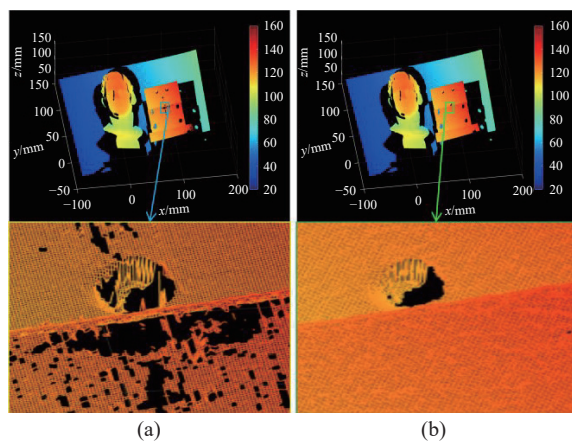


Fig. 8 HDR scene measurement experiment. (a) 3D data obtained using traditional methods. (b) 3D data obtained using the method proposed in this paper

4 Accuracy verification

4.1 Measurement of standard parts

In our experiments, we measured the metal surface with holes as shown in Fig. 9 (color online), and in order to better characterize the effectiveness

and accuracy of the proposed method, we compared it using the methods, proposed by Zhang^[15] and Liu^[26]. To ensure fairness, the methods we compared all use the three-frequency, four-step phase-shift method for wrapping phase solving.

The measurement results of the metal surface are shown in Fig. 9. The 3D result of the overexposed stripes obtained without processing is shown in Fig. 9(a), where data loss occurs in the overexposed areas. Fig. 9(b) presents the 3D point cloud data obtained using Liu's method (with three-frequency four-step phase-shifting), where the point cloud is completed in the overexposed regions; however, the accuracy is affected by low signal-to-noise ratio at the edges of channel fusion. Fig. 9(c) shows Zhang's proposed method, which effectively addresses the impact of overexposure and obtains high-quality point clouds. Compared with Zhang's method, the method in this paper (Fig. 9(d)) can realize HDR measurements in only one exposure with comparable accuracy. Compared to Liu's method, the proposed method has higher measurement accuracy in the overexposed region.

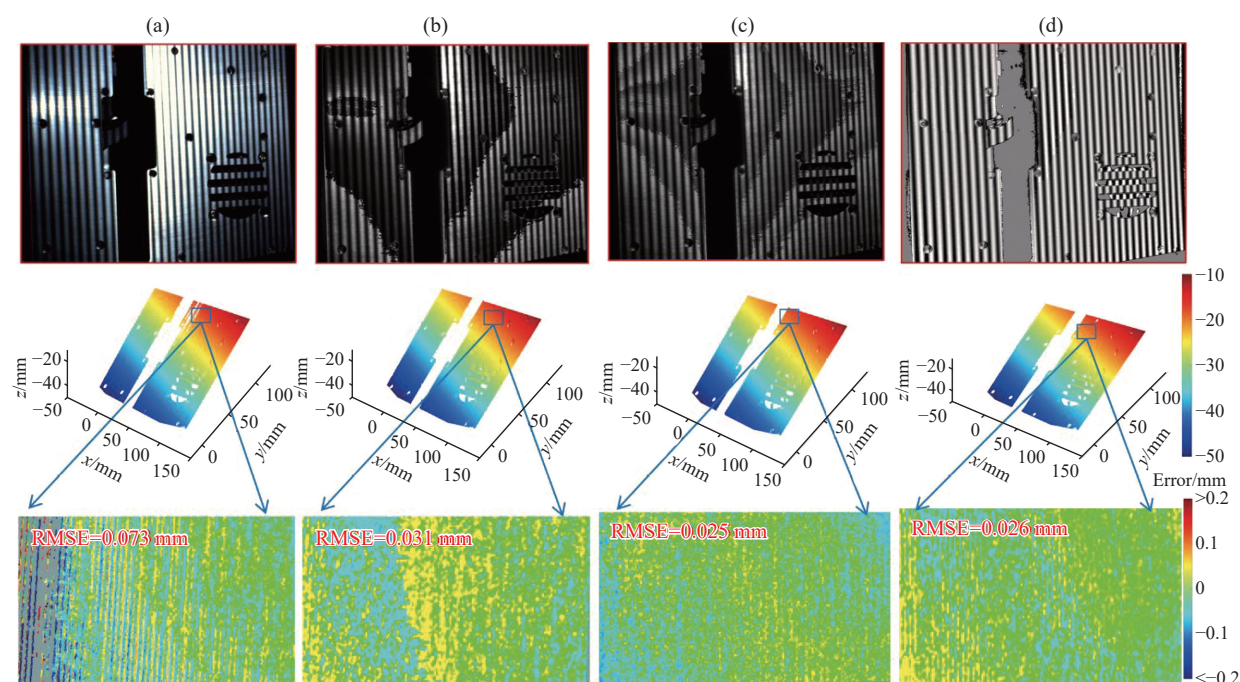


Fig. 9 Comparison of measurement results. (a) 3D data acquired by the traditional method. (b) 3D data acquired by Liu's method^[26]. (c) 3D data acquired by Zhang's proposed method^[15]. (d) 3D data acquired by the method in this paper

To quantitatively evaluate the proposed method, tests were conducted on the metal artificial standard step shown in Fig. 10(a) (color online). To better describe the effectiveness and accuracy of the proposed method, we compared it with Liu's method^[26] and traditional methods. The reconstructed 3D results are shown in Fig. 10(a)–(c) (color online). The results of plane fitting for one of the steps are illustrated in the R1, R2, and R3 regions in Fig. 10(d) (color online). The proposed method achieved an RMSE of 0.029 mm at the step, which is a 21.6% improvement in accuracy compared to Liu's method. The error distribution indicates that the point cloud is smoother and has smaller errors at the junctions of channel transformations.

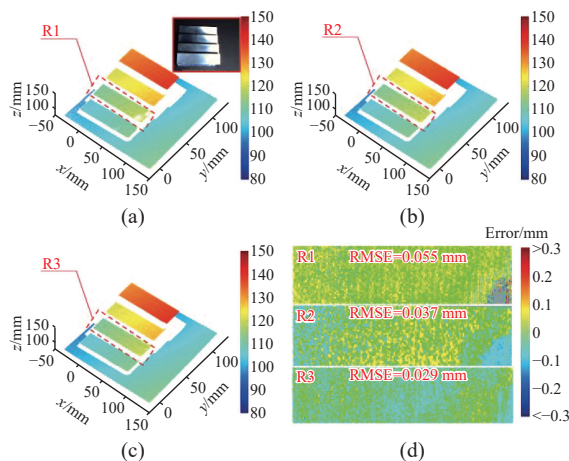


Fig. 10 Highly reflective standards and step measurement result. (a) 3D data obtained by the traditional method. (b) 3D data obtained by Liu's method^[26]. (c) 3D data obtained by the method in this paper. (d) Planar RMSEs of the three methods

To quantitatively evaluate the accuracy of the method, the 3D data of each step surface was fitted

into different step planes, and the average distance from the point on the step plane to the neighboring step planes was used as the step height. The comparison between the method in this paper and Liu's method is shown in Table 2. The accuracy is improved by 44.6% (13 μm) compared to Liu's method.

Tab. 2 Comparison of measurement accuracy

Step distance (mm)	Liu ^[26]		proposed method	
	values	errors	values	errors
12.053	12.094	0.041	12.070	0.017
10.006	10.040	0.034	10.029	0.023
8.018	7.991	0.027	8.002	0.016
6.016	5.999	0.017	6.026	0.010

4.2 Measurement efficiency

To evaluate the efficiency of the measurement methods, several existing methods were compared, with the metal plane in Section 4.1 being measured, and the results are shown in Table 3. Compared to Zhang's method, while the measurement accuracy is nearly the same, the number of images required by the proposed method is 14, a reduction of 70.8% compared to Zhang's 48 images. Compared to Liu's method, the proposed method demonstrates higher accuracy in the channel transformation alternating regions, with a 16.1% reduction in RMSE in the measured scene, and a 37.0% increase in point cloud quantity compared to traditional methods. The comparison results indicate that the proposed method ensures the completeness of HDR scene measurement data while balancing speed and accuracy.

Tab. 3 Comparison of the proposed method with the latest multi-exposure methods

	Traditional	Wang ^[5]	Liu ^[26]	Zhang ^[15]	proposed
Number of exposure times	1	3	1	4	1
Number of captured images	12	13×3+1=40	12+1=13	12×4=48	12+2=14
Number of point clouds	989 260	—	1 022 294	1 026 280	1 025 844
RMSE (mm)	0.073	—	0.031	0.025	0.026

5 Conclusion

A novel method for projector modulation is proposed, this method utilizes the independently controllable characteristics of the three channels of the color projector, avoiding the cumbersome operations of modifying stripe brightness and changing image brightness through multiple exposures with the camera. It has the advantage of obtaining the 3D

shape of HDR targets with a single exposure, thereby improving measurement speed while ensuring accuracy compared to multi-exposure methods. The experiments show that the number of images acquired is reduced by 70.8% compared to the multi-exposure method. The absolute average error of the measurement of the standard highly reflective parts is less than 0.02 mm, which represents a 44.6% decrease compared to the average error of the existing method.

References:

- [1] YANG SH CH, HUANG H L, WU G X, *et al.*. High-speed three-dimensional shape measurement with inner shifting-phase fringe projection profilometry[J]. *Chinese Optics Letters*, 2022, 20(11): 112601.
- [2] ZHENG ZH J, GAO J, ZHANG L Y, *et al.*. A novel defocus-degree-based phase unwrapping and fusion algorithm for high-speed and large-depth-range 3D measurement[J]. *IEEE Transactions on Industrial Electronics*, 2023, 70(4): 4278-4288.
- [3] 莫彩利, 王立忠, 任茂栋, 等. 小尺寸零件的无标志点扫描测量方法[J]. *中国光学 (中英文)*, 2024, 17(2): 409-422.
MO C L, WANG L ZH, REN M D, *et al.*. Scanning measurement method of small size parts without marks[J]. *Chinese Optics*, 2024, 17(2): 409-422. (in Chinese).
- [4] ZUO CH, FENG SH J, HUANG L, *et al.*. Phase shifting algorithms for fringe projection profilometry: a review[J]. *Optics and Lasers in Engineering*, 2018, 109: 23-59.
- [5] WANG ZH Y, LI K, GAO N, *et al.*. High dynamic range 3D shape measurement based on crosstalk characteristics of a color camera[J]. *Optics Express*, 2023, 31(23): 38318-38333.
- [6] SONG ZH, JIANG H L, LIN H B, *et al.*. A high dynamic range structured light means for the 3D measurement of specular surface[J]. *Optics and Lasers in Engineering*, 2017, 95: 8-16.
- [7] 刘泽隆, 李茂月, 卢新元, 等. 高动态范围条纹结构光在机检测技术及应用进展[J]. *中国光学 (中英文)*, 2024, 17(1): 1-18.
LIU Z L, LI M Y, LU X Y, *et al.*. On-machine detection technology and application progress of high dynamic range fringe structured light[J]. *Chinese Optics*, 2024, 17(1): 1-18. (in Chinese).
- [8] RI SH E, FUJIGAKI M, MORIMOTO Y. Intensity range extension method for three-dimensional shape measurement in phase-measuring profilometry using a digital micromirror device camera[J]. *Applied Optics*, 2008, 47(29): 5400-5407.
- [9] NIU B, QU X H, GUAN X M, *et al.*. Rapid detection of highly reflective surface defects based on digital micromirror device[J]. *Optics Communications*, 2021, 501: 127385.
- [10] HUANG H ZH, NIU B, CHENG S, *et al.*. Adaptive pixel-by-pixel modulated 3-D morphometry based on digital micromirror device[J]. *IEEE Transactions on Instrumentation and Measurement*, 2024, 73: 5012010.
- [11] SURESH V, WANG Y J, LI B W. High-dynamic-range 3D shape measurement utilizing the transitioning state of digital micromirror device[J]. *Optics and Lasers in Engineering*, 2018, 107: 176-181.
- [12] ZHANG S. Rapid and automatic optimal exposure control for digital fringe projection technique[J]. *Optics and Lasers in Engineering*, 2020, 128: 106029.
- [13] ZHANG L, CHEN Q, ZUO CH, *et al.*. Real-time high dynamic range 3D measurement using fringe projection[J]. *Optics Express*, 2020, 28(17): 24363-24378.
- [14] WANG J H, ZHOU Y G, YANG Y X. A novel and fast three-dimensional measurement technology for the objects surface with non-uniform reflection[J]. *Results in Physics*, 2020, 16: 102878.
- [15] ZHANG S, YAU S T. High dynamic range scanning technique[J]. *Optical Engineering*, 2009, 48(3): 033604.
- [16] WANG J H, YANG Y X. A new method for high dynamic range 3D measurement combining adaptive fringe projection and original-inverse fringe projection[J]. *Optics and Lasers in Engineering*, 2023, 163: 107490.

- [17] WANG J H, XU P, SHAO M W, et al.. High dynamic range 3D shape reconstruction: combination of adaptive fringe intensity, iterative exposure time adjustment and least quadratic curve fitting[J]. *Optik*, 2024, 307: 171813.
- [18] SUN J H, ZHANG Q Y. A 3D shape measurement method for high-reflective surface based on accurate adaptive fringe projection[J]. *Optics and Lasers in Engineering*, 2022, 153: 106994.
- [19] LIU Y ZH, FU Y J, CAI X Q, et al.. A novel high dynamic range 3D measurement method based on adaptive fringe projection technique[J]. *Optics and Lasers in Engineering*, 2020, 128: 106004.
- [20] LIN H, GAO J, MEI Q, et al.. Adaptive digital fringe projection technique for high dynamic range three-dimensional shape measurement[J]. *Optics Express*, 2016, 24(7): 7703-7718.
- [21] LI M H, CAO Y P, WU H T. Three-dimensional reconstruction for highly reflective diffuse object based on online measurement[J]. *Optics Communications*, 2023, 533: 129276.
- [22] HU Y, CHEN Q, LIANG Y CH, et al.. Microscopic 3D measurement of shiny surfaces based on a multi-frequency phase-shifting scheme[J]. *Optics and Lasers in Engineering*, 2019, 122: 1-7.
- [23] 冯维, 徐仕楠, 王恒辉, 等. 逐像素调制的高反光表面三维测量方法[J]. *中国光学*, 2022, 15(3): 488-497.
FENG W, XU SH N, WANG H H, et al.. Three-dimensional measurement method of highly reflective surface based on per-pixel modulation[J]. *Chinese Optics*, 2022, 15(3): 488-497. (in Chinese).
- [24] 冯维, 汤少靖, 赵晓冬, 等. 基于自适应条纹的高反光表面三维面形测量方法[J]. *光学学报*, 2020, 40(5): 0512003.
FENG W, TANG SH J, ZHAO X D, et al.. Three-dimensional shape measurement method of high-reflective surfaces based on adaptive fringe-pattern[J]. *Acta Optica Sinica*, 2020, 40(5): 0512003. (in Chinese).
- [25] CAI X X, XU R H, LI H, et al.. High-reflective surfaces shape measurement technology based on adaptive fringe projection[J]. *Sensors and Actuators A: Physical*, 2022, 347: 113916.
- [26] LIU Y ZH, FU Y J, ZHUAN Y H, et al.. High dynamic range real-time 3D measurement based on Fourier transform profilometry[J]. *Optics & Laser Technology*, 2021, 138: 106833.
- [27] OTI E U, OLUSOLA M O, EZE F C, et al.. Comprehensive review of K-means clustering algorithms[J]. *International Journal of Advances in Scientific Research and Engineering*, 2021, 7(8): 64-69.
- [28] LAI B Y, CHIANG P J. Improved structured light system based on generative adversarial networks for highly-reflective surface measurement[J]. *Optics and Lasers in Engineering*, 2023, 171: 107783.
- [29] IKOTUN A M, EZUGWU A E, ABUALIGAH L, et al.. K-means clustering algorithms: a comprehensive review, variants analysis, and advances in the era of big data[J]. *Information Sciences*, 2023, 622: 178-210.

Author Biographies:



HUANG Hao-zhen (1994—), male, born in Xiangcheng, Henan Province, received the B.S. and M.S. degrees from Tiangong University, in 2018 and 2021, respectively, and is currently pursuing the Ph.D. degree in Instrument Science and Technology at Tianjin University. His main research focuses on optical three-dimensional measurement. E-mail: huanghaozhen0913@126.com



ZHANG Fu-min (1982—), male, born in Tianjin, Ph.D, Professor, School of Precision Instrument and Opto-electronics Engineering, Tianjin University. He has long been engaged in the research and industrial application of key technologies related to visual 3D measurement and laser measurement. E-mail: zhangfumin@tju.edu.cn